optica

Demonstration of a non-Abelian geometric controlled-NOT gate in a superconducting circuit

Kai Xu,[1,2] Wen Ning,[3] Xin-Jie Huang,[3] Pei-Rong Han,[3] Hekang Li,[2] Zhen-Biao Yang,[3,4] Dongning Zheng,[1,2] Heng Fan,[1,2,5] and Shi-Biao Zheng[3,6]

[1]Institute of Physics and Beijing National Laboratory for Condensed Matter Physics, Chinese Academy of Sciences, Beijing 100190, China
[2]CAS Center for Excellence in Topological Quantum Computation, University of Chinese Academy of Sciences, Beijing 100190, China
[3]Fujian Key Laboratory of Quantum Information and Quantum Optics, College of Physics and Information Engineering, Fuzhou University, Fuzhou, Fujian 350108, China
[4]e-mail: zbyang@fzu.edu.cn
[5]e-mail: hfan@iphy.ac.cn
[6]e-mail: t96034@fzu.edu.cn

Received 30 November 2020; revised 25 April 2021; accepted 4 June 2021 (Doc. ID 416264); published 28 June 2021

Holonomies, arising from non-Abelian geometric transformations of quantum states in Hilbert space, offer a promising way for quantum computation. These holonomies are not commutable and thus can be used for the realization of a universal set of quantum logic gates, where the global geometric feature may result in some noise-resilient advantages. Here we report, to our knowledge, the first on-chip realization of a non-Abelian geometric controlled-NOT gate in a superconducting circuit, which is a building block for constructing a holonomic quantum computer. The conditional dynamics is achieved in an all-to-all connected architecture involving multiple frequency-tunable superconducting qubits controllably coupled to a resonator; a holonomic gate between any two qubits can be implemented by tuning their frequencies on-resonance with the resonator and applying a two-tone drive to one of them. This gate represents an important step towards the all-geometric realization of scalable quantum computation on a superconducting platform. © 2021 Optical Society of America under the terms of the OSA Open Access Publishing Agreement

https://doi.org/10.1364/OPTICA.416264

1. INTRODUCTION

When a nondegenerate quantum system makes a cyclic evolution in the Hilbert space, it will pick up a phase, which, in general, is contributed by both the dynamical and geometric effects. The dynamical part is the time integral of the energy, while the geometric one depends upon the area enclosed by the loop that the quantum state traverses in the Hilbert space. This effect, discovered by Berry in cyclic and adiabatic evolutions [1], has been generalized to nonadiabatic [2] and degenerate [3] cases. If a system has degenerate energy levels, the cyclic evolution of the corresponding degenerate subspaces will produce a matrix-valued quantum state transformation that is path dependent and referred to as non-Abelian geometric phase or holonomy [3]. The Berry phase and holonony depend upon the global geometry of the associated loops and have intrinsic resistance to certain kinds of small errors, suggesting that quantum gates based on geometric operations have practical advantages as compared to dynamical gates [4–7]. In particular, it was shown that all of the elementary one- and two-qubit gates needed for accomplishing any quantum computation task could be achieved with Berry phase and holonomic transformations, offering a possibility for implementations of geometric quantum computation [8,9].

The conditional Berry phase was first observed in nuclear magnetic resonance systems [10]. However, the relatively long operation time associated with an adiabatic evolution represents an unfavorable condition for the implementation of geometric quantum computation with such controlled phase gates. As such, geometric effects without the adiabatic restriction are highly desirable for the implementation of quantum logic gates that are robust against noises [11–16]. So far, nonadiabatic geometric controlled-phase gates have been realized in ion traps [17–20] and superconducting circuits [21–23]. On the other hand, Sjöqvist *et al.* have proposed an approach for realizing a universal set of elementary gates based on nonadiabatic holonomies [24], whose robustness against noises has been analyzed [25,26]. Following this approach, a universal gate set involving two non-commutable single-qubit gates and a two-qubit controlled-NOT (CNOT) gate have been experimentally realized with nuclear magnetic resonance [27] and solid-state spins [28,29]. Several groups have demonstrated holonomic single-qubit gates in superconducting circuits [30–33], which represent a promising platform for quantum computation [34]. Recently, Egger *et al.* reported a holonomic operation for producing entangled states in a superconducting circuit [35]. However, a non-Abelian geometric entangling gate necessary for constructing a universal holonomic gate set has not been implemented in such scalable systems. More recently, Han *et al.* reported a universal set of time-optimal geometric gates with

superconducting qubits [36], where single-qubit gates were realized using non-Abelian geometric phase, but the two-qubit gate was based on Abelian geometric phase.

In this paper, we propose and experimentally demonstrate a scheme for realizing a non-adiabatic, non-Abelian geometric CNOT gate for two qubits, one acting as the control qubit and the other as the target qubit. The two qubits are strongly coupled to a resonator, so that the energy levels of the target qubit depend on the state of the control qubit. This conditional energy-level shift enables the target qubit to be resonantly driven by classical fields, conditional on the state of the control qubit. With a suitable setting of the parameters, these classical fields can drive the degenerate subspace spanned by the two basis states of the target qubit to undergo a conditional cyclic evolution, realizing a CNOT gate between these two qubits. We realize this holonomic gate in a superconducting multi-qubit processor, where any two qubits can be selectively coupled to a common resonator but effectively decoupled from other qubits through frequency tuning. This flexibility enables direct implementation of holonomic gates between any pair of qubits on the chip, without the restriction of nearest-neighbor couplings. The measured process fidelity for the CNOT gate is above 0.9. With further improvements in the device design and fabrication, as confirmed by our numerical simulations, the gate fidelity can be significantly increased. Our scheme is applicable to other spin-boson systems, such as cavity QED and ion traps [37].

2. THEORETICAL MODEL

The system under consideration is composed of two qutrits coupled to a resonator. Each qutrit has three basis states, as shown in Fig. 1(a), with $|g\rangle$ and $|f\rangle$ serving as two logic states of a qubit, and $|e\rangle$, lying between $|g\rangle$ and $|f\rangle$, used as an auxiliary state for realizing the controlled logic operation. For simplicity, we will refer to the qutrits as qubits. As will be shown, the control qubit (Q_1) remains in its computational space, while the target qubit (Q_2) has a probability of being populated in the auxiliary level $|e\rangle$ during the gate operation. The transition $|g\rangle \leftrightarrow |e\rangle$ of each qubit resonantly interacts with the resonator, while $|f\rangle$ state is effectively decoupled from the resonator. In the interaction picture, the Hamiltonian describing the qubit–resonator interaction is given by

$$H_{\rm int} = \hbar \sum_{j=1}^{2} \lambda_j \left(a|e_j\rangle\langle g_j| + a^\dagger |g_j\rangle\langle e_j| \right), \tag{1}$$

where a and $a^\dagger$ are the photonic annihilation and creation operators for the resonator, respectively, and λ_j is the coupling strength between the jth qubit and the resonator with angular frequency ω_r. We here have set the energy of the ground state $|g\rangle$ for each qubit to be zero. To realize the CNOT gate, the transition $|g_2\rangle \leftrightarrow |e_2\rangle$ of Q_2 is driven by a classical field with angular frequency $(\omega_r - \lambda_2)$, and $|e_2\rangle \leftrightarrow |f_2\rangle$ is driven by a classical field with angular frequency $(\omega_{f,2} - \omega_r + \lambda_2)$, where $\hbar\omega_{f,2}$ is the energy of Q_2's state $|f_2\rangle$ [Fig. 1(a)]. The interaction between the second qubit and the driving fields is described by

$$H_{\rm dr} = \hbar \left[\Omega_{ge} e^{i\lambda_2 t} |e_2\rangle\langle g_2| - \Omega_{ef} e^{-i\lambda_2 t} |f_2\rangle\langle e_2| \right] + \text{h.c.}, \tag{2}$$

where Ω_{ge} and Ω_{ef} denote the Rabi frequencies of the two fields driving $|g_2\rangle \leftrightarrow |e_2\rangle$ and $|e_2\rangle \leftrightarrow |f_2\rangle$, respectively. We here have assumed that the phases of the fields driving the transitions $|g\rangle \leftrightarrow |e\rangle$ and $|e\rangle \leftrightarrow |f\rangle$ are zero and π, respectively.

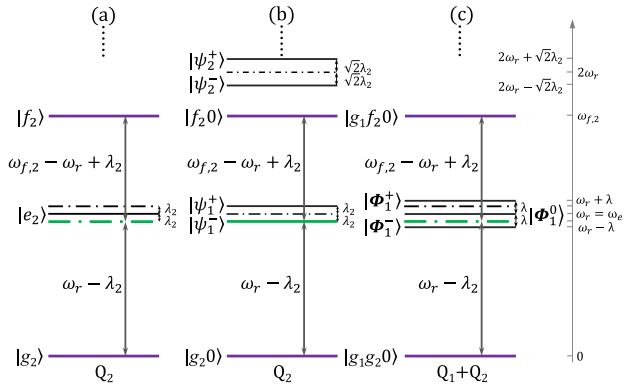

Fig. 1. Energy level configuration and excitation scheme for the two-qubit CNOT gate. The control and target qubits are denoted as Q_1 and Q_2, respectively. (a) Bare energy levels of Q_2 and frequencies of the drives. The quantum information of each qubit is encoded in states $|g\rangle$ and $|f\rangle$, with the auxiliary state $|e\rangle$ used for realizing the controlled-NOT gate. The transitions $|g_2\rangle \leftrightarrow |e_2\rangle$ and $|e_2\rangle \leftrightarrow |f_2\rangle$ of Q_2 are driven by classical fields of angular frequencies $(\omega_r - \lambda_2)$ and $(\omega_{f,2} - \omega_r + \lambda_2)$, respectively. Here ω_r is the angular frequency of the resonator that is strongly coupled to $|g_2\rangle \leftrightarrow |e_2\rangle$ with the coupling strength λ_2, and $\hbar\omega_{f,2}$ is the energy spacing between $|f_2\rangle$ and $|g_2\rangle$. (b) Dressed states and energy levels with Q_1 initially in $|f_1\rangle$. When being initially in $|f_1\rangle$, Q_1 is effectively decoupled from the resonator due to the large detuning. The strong coupling between Q_2 and the resonator results in dressed states $|\psi_n^\pm\rangle$, whose energy levels are nonlinearly dependent on the coupling strength. The two driving fields are on-resonance with the transitions $|g_2 0\rangle \leftrightarrow |\psi_1^-\rangle$ and $|\psi_1^-\rangle \leftrightarrow |f_2 0\rangle$, respectively, but highly detuned from other transitions. (c) Dressed states and energy levels with Q_1 initially in $|g_1\rangle$. If initially in $|g_1\rangle$, Q_1, together with Q_2, is strongly coupled to the resonator, resulting in three dressed states $|\Phi_1^\pm\rangle$ and $|\Phi_1^0\rangle$ in the single-excitation subspace. The driving fields are highly detuned from transitions of $|g_1 g_2 0\rangle$ and $|g_1 f_2 0\rangle$ to these dressed states.

The strong couplings between the qubits and the resonator produce dressed states, whose energy levels depend on the total excitation number as well as on the number of qubits being initially populated in $|g\rangle$. When the control qubit is in the state $|f_1\rangle$, it does not interact with the resonator, and the coupling between the target qubit and the resonator is described by the Jaynes–Cummings model, whose eigenstates are given by

$$|\psi_0\rangle = |g_2 0\rangle, \tag{3}$$

$$|\psi_n^\pm\rangle = \frac{1}{\sqrt{2}} \left(|e_2(n-1)\rangle \pm |g_2 n\rangle \right), \; n \geq 1. \tag{4}$$

Here the second symbol in each ket denotes the photon number in the resonator. The eigenenergies of the dressed states $|\psi_n^\pm\rangle$ are $\hbar(n\omega_r \pm \sqrt{n}\lambda_2)$. We here consider the case that the resonator is initially in the vacuum state $|0\rangle$. Consequently, the classical fields resonantly couple states $|g_2 0\rangle$ and $|f_2 0\rangle$ to the single-excitation dressed state $|\psi_1^-\rangle$, as sketched in Fig. 1(b). We suppose that Ω_{ge} and Ω_{ef} are much smaller than λ_2, so that the classical fields cannot drive the transitions from $|\psi_1^-\rangle$ to $|\psi_2^\pm\rangle$ due to the large detunings. However, these off-resonant couplings shift the energy levels of $|\psi_1^-\rangle$ by $-2\hbar\delta_1$, with $\delta_1 = 2\Omega_{ge}^2/\lambda_2$ (see Supplement 1). Furthermore, off-resonant coupling to $|h_1\rangle|g_2 0\rangle$ and $|e_1\rangle|\psi_2^\pm\rangle$ shifts the energy level of $|f_1\rangle|\psi_1^\pm\rangle$ by an amount of $-\hbar\delta_2$, where $\delta_2 = 9\lambda_1^2/4\alpha_1$ (see Supplement 1), and $|h_1\rangle$ is the fourth level of Q_1, and α_1 is its anharmonicity ($\alpha_j = 2\omega_{e,j} - \omega_{f,j}$, $j = 1, 2$). To

compensate for these shifts, the angular frequency of the field driving $|g_2\rangle \leftrightarrow |e_2\rangle$ should be set to $\omega_{d,1} = \omega_r - \lambda_2 - \delta_1 - \delta_2$, while that of the field driving $|e_2\rangle \leftrightarrow |f_2\rangle$ should be set to $\omega_{d,2} = \omega_{f,2} - \omega_r + \lambda_2 + \delta_1 + \delta_2$. With this setting and performing the transformation $\exp(iH_{\rm int}t/\hbar)$, the system dynamics associated with Q_1's state $|f_1\rangle$ can be described by the effective Hamiltonian

$$H_{\rm eff} = \hbar\Omega\left[\cos\frac{\phi}{2}|g_20\rangle\langle\psi_1^-| + \sin\frac{\phi}{2}|f_20\rangle\langle\psi_1^-|\right]|f_1\rangle\langle f_1| + \text{h.c.}, \tag{5}$$

where

$$\Omega = \sqrt{\Omega_{ge}^2 + \Omega_{ef}^2}/\sqrt{2}, \tag{6}$$

$$\tan\frac{\phi}{2} = \Omega_{ef}/\Omega_{ge}. \tag{7}$$

When Q_1 is initially in the state $|g_1\rangle$, it is also strongly coupled to the resonator, and there are three dressed states in the single-excitation subspace:

$$|\Phi_1^0\rangle = (-\sin\theta|e_1g_20\rangle + \cos\theta|g_1e_20\rangle), \tag{8}$$

$$|\Phi_1^\pm\rangle = \frac{1}{\sqrt{2}}[(\cos\theta|e_1g_20\rangle + \sin\theta|g_1e_20\rangle) \pm |g_1g_21\rangle], \tag{9}$$

where $\tan\theta = \lambda_2/\lambda_1$. The corresponding eigenenergies are $\hbar\omega_e$ and $\hbar(\omega_e \pm \sqrt{\lambda_1^2+\lambda_2^2})$, as shown in Fig. 1(c). When $(\sqrt{\lambda_1^2+\lambda_2^2} - \lambda_2)$ is much larger than Ω_{ge} and Ω_{ef}, the qubits cannot make any transition between either of these single-excitation dressed states and the state $|g_1g_20\rangle$ or $|g_1f_20\rangle$, as each of these transitions is highly detuned from the driving fields. As a consequence, Q_2 is not affected by the driving fields when Q_1 is initially in the state $|g_1\rangle$. Therefore, the system dynamics is described by the effective Hamiltonian of Eq. (5). The evolution of the initial basis states $|c_1d_20\rangle$ $(c, d = g, f)$ are given by

$$|\psi_{cd}(t)\rangle = \exp\left(-i\int_0^t H_{\rm eff}dt/\hbar\right)|c_1d_20\rangle. \tag{10}$$

When Ω_{ef}/Ω_{ge} remains unchanged during the interaction, the evolution satisfies the parallel-transport condition $\langle\psi_{cd}(t)|H_{\rm eff}|\psi_{c'd'}(t)\rangle = 0$, and hence is purely geometric. If the Rabi frequencies of the driving fields and the interaction time are appropriately chosen so that $\int_0^T \Omega dt = \pi$, the degenerate qubit subspace undergoes a cyclic evolution. Consequently, the qubits return to the computational space $\{|g_1g_2\rangle, |g_1f_2\rangle, |f_1g_2\rangle, |f_1f_2\rangle\}$ with the resonator left in the vacuum state $|0\rangle$ after the time T. With this setting, the evolution operator of the qubits in the computational basis is

$$U = \begin{pmatrix} 1 & 0 & 0 & 0 \\ 0 & 1 & 0 & 0 \\ 0 & 0 & -\cos\phi & \sin\phi \\ 0 & 0 & \sin\phi & \cos\phi \end{pmatrix}, \tag{11}$$

which is a non-Abelian holonomy. For $\phi = \pi/2$, i.e., $\Omega_{ge} = \Omega_{ef}$, this corresponds to a CNOT gate, which flips the state of the target qubit conditional on the control qubit being in the state $|f_1\rangle$.

3. EXPERIMENTAL IMPLEMENTATION

The experiment is performed in a superconducting circuit involving five frequency-tunable qubits, labeled from Q_1 to Q_5, coupled to a resonator with a fixed frequency $\omega_r/2\pi = 5.584$ GHz [21,38,39]. In our experiment, Q_1 and Q_2, whose anharmonicities are $2\pi \times 242$ MHz and $2\pi \times 249$ MHz, are used as the control and target qubits, respectively. The on-resonance coupling strengths of the $g-e$ transitions of Q_1 and Q_2 to the resonator are respectively $\lambda_1 = 2\pi \times 20.8$ MHz and $\lambda_2 = 2\pi \times 19.9$ MHz. The energy relaxation time T_1 and pure Gaussian dephasing time T_2^* for the basis state $|f\rangle$ of Q_1 (Q_2) are 13.0 (10.7) μs and 2.1 (1.5) μs, while those for the intermediate state $|e\rangle$ are 23.9 (15.9) μs and 2.7 (2.1) μs, respectively. The other qubits are on far off-resonance with the resonator so that their interactions with the resonator are effectively switched off throughout the gate operation. We note that during the gate operation, the two qubits have a probability of being populated in $|f_1e_2\rangle$, which is significantly coupled to $|e_1f_2\rangle$ via virtual photon exchange, as the two qubits almost have the same anharmonicity $\alpha \simeq 2\pi \times 240$ MHz. To suppress this coupling, Q_1 should be detuned from Q_2 by an amount much larger than $\lambda_1\lambda_2/\alpha$. This detuning slightly changes the energy level configuration of the dressed states associated with Q_1's initial state $|g_1\rangle$, but does not affect the gate dynamics.

As shown in Fig. 2, the experiment starts with the initialization of Q_1 and Q_2 to the ground state $|g\rangle$ at their idle frequencies 5.47 GHz and 5.43 GHz, respectively, which is followed by the preparation of each qubit in one of the six states $\{|g\rangle, (|g\rangle - i|f\rangle)/\sqrt{2}, (|g\rangle + i|f\rangle)/\sqrt{2}, (|g\rangle + |f\rangle)/\sqrt{2}, (|g\rangle - |f\rangle)/\sqrt{2}, |f\rangle\}$. Except $|g\rangle$, each of the other single-qubit states is produced by a $g-e$ $\pi/2$- or π-pulse followed by a $e-f$ π-pulse.

After these effective single-qubit rotations, these two qubits are prepared in a product state. We then apply square Z pulses to both qubits, tuning their $|g\rangle \leftrightarrow |e\rangle$ transition frequencies to 5.58 GHz and 5.584 GHz and thus switching on their interactions with the resonator. Accompanying these Z pulses, a driving pulse composed of two components with frequencies of 5.565 GHz and 5.369 GHz is applied to Q_2, resonantly connecting the computational states $|g_20\rangle$ and $|f_20\rangle$ to the dressed state $|\psi_1^-\rangle$. The Rabi frequencies of these driving fields are $\Omega_{ge} = \Omega_{ef} = 2\pi \times 2.2$ MHz. Since the resonator is initially in the vacuum state, the system dynamics is governed by the effective Hamiltonian (5) and the time evolution

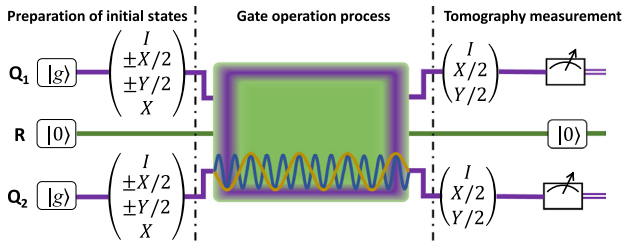

Fig. 2. Pulse sequence. Before the gate operation, both qubits are initialized to their ground states at the corresponding idle frequencies, where single-qubit rotations are performed to prepare them in a product state. Then a Z pulse is applied to Q_1, tuning $|g_1\rangle \leftrightarrow |e_1\rangle$ close to the resonator's frequency; Q_2 is subjected to a Z pulse, which brings $|g_2\rangle \leftrightarrow |e_2\rangle$ to the resonator's frequency, and a driving pulse involving two frequency components on-resonance with the transitions $|g_20\rangle \leftrightarrow |\psi_1^-\rangle$ and $|\psi_1^-\rangle \leftrightarrow |f_20\rangle$. After the CNOT gate, realized with these pulses, both qubits are tuned back to their idle frequencies for quantum state tomography.

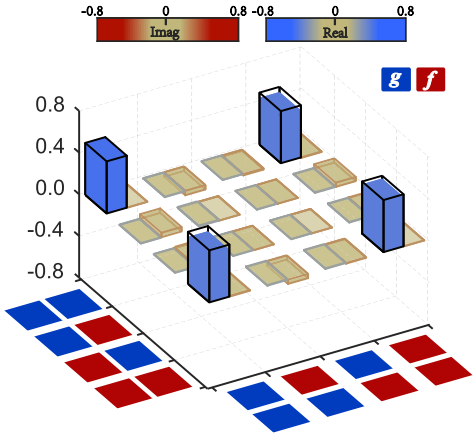

Fig. 3. Measured density matrix of the output state with the input state $(|g_1g_2\rangle + |f_1g_2\rangle)/\sqrt{2}$. Each matrix element is characterized by two colorbars, one for the real part and the other for the imaginary part. The black wire frames denote the matrix elements of the ideal output states.

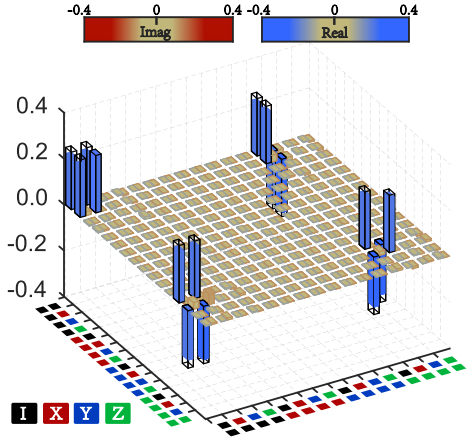

Fig. 4. Measured process matrix for the realized CNOT gate. The process matrix is measured by preparing a set of 36 distinct input product states in the computational basis $\{|g_1g_2\rangle, |g_1f_2\rangle, |f_1g_2\rangle, |f_1f_2\rangle\}$ and reconstructing the density matrices for these states and for the output states produced by the CNOT gate. The $|e\rangle$-state populations of Q_1 and Q_2, averaged over the 36 output states, are 2.2% and 2.8%, respectively.

given by Eq. (10). After a duration of $\tau = 205$ ns, the CNOT gate is realized.

One of the most important features of the CNOT gate is that it can convert a two-qubit product state into an entangled state. In particular, when the control qubit is initially in the superposition state $(|g_1\rangle + |f_1\rangle)/\sqrt{2}$ and the target state in $|g_2\rangle$, they will evolve to the maximally entangled state $(|g_1g_2\rangle + |f_1f_2\rangle)/\sqrt{2}$ after this gate. We measure this output state by quantum state tomography. This is realized by subsequently biasing each of the two qubits back to its idle frequency right after the gate operation, applying an $e-f$ π-pulse to each qubit, and measuring its state along one of the three orthogonal (x, y, and z) axes of the corresponding Bloch sphere with respect to the basis $\{|g\rangle, |e\rangle\}$. The z measurement is directly realized by state readout, while the x (y) measurement is realized by the combination of a $g-e$ $\pi/2$-pulse and state readout. The reconstructed output two-qubit density matrix is displayed in Fig. 3, which has a fidelity of 0.935 ± 0.016 to the ideal maximally entangled state, and a concurrence of 0.888 ± 0.029.

To fully characterize the performance of the implemented CNOT gate, we prepare a full set of 36 distinct two-qubit input states before the two-qubit gates, and measure these states and the corresponding output states. With these measured results, the process matrix for the gate operation is reconstructed. The measured process matrix, $\chi_{\rm meas}$, is presented in Fig. 4. The gate fidelity, defined as $F = tr(\chi_{\rm id}\chi_{\rm meas})$, is 0.905 ± 0.008, where $\chi_{\rm id}$ is the ideal process matrix. The measured fidelity is in good agreement with the numerical simulation based on the Lindblad master equation, which yields a fidelity of 0.908. One of the error sources is the transitions from $|g_1g_20\rangle$ and $|g_1f_20\rangle$ to $|\Phi_1^0\rangle$ and $|\Phi_1^{\pm}\rangle$ and the transition from $|\psi_1^-\rangle$ to $|\psi_2^-\rangle$ induced by the drive, which causes quantum information leakage to the noncomputational space. Such a leakage error can be mitigated through improvement of the qubit's nonlinearity or by balancing the drive amplitude and the gate operation time provided the qubits' coherence is bettered, which allows the gate fidelity to be increased by about 6.5% (see Supplement 1). On the other hand, the qubits' energy relaxation and their dephasings contribute about 1.8% and 1.6% of the error, respectively. Our further numerical simulations show that the CNOT gate with a fidelity above 99% can be obtained with sufficiently large qubit nonlinearity α_j and qubit-resonator coupling strength λ_j. For instance, with the parameters $\lambda_j/2\pi = 110$ MHz, $\alpha_j/2\pi = -3.69$ GHz [40,41], $\Omega_{ge}/2\pi = \Omega_{ef}/2\pi = 5.9$ MHz, $T_1 = 60$ μs, and $T_{2,j}^* = 86$ μs, we find a CNOT gate with the operation time of about 87 ns and fidelity of 0.991, which is at the surface code threshold for fault tolerance [42–44]. We note this gate is robust against the frequency fluctuations of the driving fields. Suppose that the angular frequencies of these drives deviate from the desired values by an amount of $\delta\omega = 2\pi \times 100$ kHz. The infidelity incurred by this deviation is about $[\pi(\delta\omega)^2/(8\Omega_{ge/ef}^2)]^2 \simeq 0.1\%$.

4. CONCLUSION

In conclusion, we have proposed and demonstrated a scheme for implementing a non-Abelian geometric gate between two superconducting qubits, whose ground and second excited states act as the computational basis states. The conditional dynamics is realized by resonantly driving the transitions between the basis states of the target qubit to the single-excitation dressed states formed by this qubit and the resonator. This entangling gate, together with the previously demonstrated non-Abelian geometric single-qubit gates [30–33], constitutes a universal set of holonomic gates for realizing quantum computation with superconducting qubits. The method can be directly applied to other systems composed of qubits coupled to a bosonic mode, including cavity QED and ion traps.

Funding. National Natural Science Foundation of China (11674060, 11874114, 11875108, 11904393, 11934018, 92065114); the Strategic Priority Research Program of Chinese Academy of Sciences (XDB28000000); Beijing Municipal Natural Science Foundation (Z200009).

Acknowledgment. We thank Haohua Wang at Zhejiang University for technical support. S.-B.Z. conceived the experiment. K.X., W. N., and Z.-B.Y. performed the experiment and analyzed the data with the assistance of X.-J.H. and P.-R.H. H.L. and D.Z. provided the devices used for the experiment. S.-B.Z., Z.-B.Y., K.X., and H.F. wrote the manuscript with feedbacks from all authors. The experiment was performed at Fuzhou University.

Disclosures. The authors declare no conflicts of interest.

Data availability. Data underlying the results presented in this paper are not publicly available at this time but may be obtained from the authors upon reasonable request.

Supplemental document. See Supplement 1 for supporting content.

REFERENCES

1. M. V. Berry, "Quantal phase-factors accompanying adiabatic changes," Proc. R. Soc. London A **392**, 45–57 (1984).
2. Y. Aharonov and A. Anandan, "Phase change during a cyclic quantum evolution," Phys. Rev. Lett. **58**, 1593–1596 (1987).
3. F. Wilczek and A. Zee, "Appearance of gauge structure in simple dynamical systems," Phys. Rev. Lett. **52**, 2111–2114 (1984).
4. G. D. Chiara and G. M. Palma, "Berry phase for a spin 1/2 particle in a classical fluctuating field," Phys. Rev. Lett. **91**, 090404 (2003).
5. S. Filipp, J. Klepp, Y. Hasegawa, C. Plonka-Spehr, U. Schmidt, P. Geltenbort, and H. Rauch, "Experimental demonstration of the stability of Berry's phase for a spin-1/2 particle," Phys. Rev. Lett. **102**, 030404 (2009).
6. A. Carollo, I. Fuentes-Guridi, M. F. Santos, and V. Vedral, "Geometric phase in open systems," Phys. Rev. Lett. **90**, 160402 (2003).
7. S.-B. Zheng, "Geometric phase for a driven quantum field subject to decoherence," Phys. Rev. A **91**, 052117 (2015).
8. P. Zanardi and M. Rasetti, "Holonomic quantum computation," Phys. Lett. A **264**, 94–99 (1999).
9. J. Pachos, P. Zanardi, and M. Rasetti, "Non-Abelian Berry connections for quantum computation," Phys. Rev. A **61**, 010305 (2000).
10. J. A. Jones, V. Vedral, A. Ekert, and G. Castagnoli, "Geometric quantum computation with NMR," Nature (London) **403**, 869–871 (2000).
11. X.-B. Wang and M. Keiji, "Nonadiabatic conditional geometric phase shift with NMR," Phys. Rev. Lett. **87**, 097901 (2001).
12. S.-L. Zhu and Z.-D. Wang, "Implementation of universal quantum gates based on nonadiabatic geometric phases," Phys. Rev. Lett. **89**, 097902 (2002).
13. A. Nazir, T. Spiller, and W. J. Munro, "Decoherence of geometric phase gates," Phys. Rev. A **65**, 042303 (2002).
14. A. Blais and A.-M. S. Tremblay, "Effect of noise on geometric logic gates for quantum computation," Phys. Rev. A **67**, 012308 (2003).
15. J. Zhang, S. J. Devitt, J. Q. You, and F. Nori, "Holonomic surface codes for fault-tolerant quantum computation," Phys. Rev. A **97**, 022335 (2018).
16. Y.-H. Chen, W. Qin, R. Stassi, X. Wang, and F. Nori, "Generation of Fock-state superpositions and binomial-code holonomic gates via dressed intermediate states in the ultrastrong light-matter coupling regime," arXiv:2012.06090 (2021).
17. D. Leibfried, B. DeMarco, V. Meyer, D. Lucas, M. Barrett, J. Britton, W. M. Itano, B. Jelenković, C. Langer, T. Rosenband, and D. J. Wineland, "Experimental demonstration of a robust, high-fidelity geometric two ion-qubit phase gate," Nature (London) **422**, 412–415 (2003).
18. J. Benhelm, G. Kirchmair, C. F. Roos, and R. Blatt, "Towards fault-tolerant quantum computing with trapped ions," Nat. Phys. **4**, 463–466 (2008).
19. C. J. Ballance, T. P. Harty, N. M. Linke, M. A. Sepiol, and D. M. Lucas, "High-fidelity quantum logic gates using trapped-ion hyperfine qubits," Phys. Rev. Lett. **117**, 060504 (2016).
20. J. P. Gaebler, T. R. Tan, Y. Lin, Y. Wan, R. Bowler, A. C. Keith, S. Glancy, K. Coakley, E. Knill, D. Leibfried, and D. J. Wineland, "High-fidelity universal gate set for $^{9}Be^{+}$ ion qubits," Phys. Rev. Lett. **117**, 060505 (2016).
21. C. Song, S.-B. Zheng, P. Zhang, K. Xu, L. Zhang, Q. Guo, W. Liu, D. Xu, H. Deng, K. Huang, D. Zheng, X. Zhu, and H. Wang, "Continuous-variable geometric phase and its manipulation for quantum computation in a superconducting circuit," Nat. Commun. **8**, 1061 (2017).
22. Y. Xu, Z. Hua, T. Chen, X. Pan, X. Li, J. Han, W. Cai, Y. Ma, H. Wang, Y. P. Song, Z.-Y. Xue, and L. Sun, "Experimental implementation of universal nonadiabatic geometric quantum gates in a superconducting circuit," Phys. Rev. Lett. **124**, 230503 (2020).
23. Y. Xu, Y. Ma, W. Cai, X. Mu, W. Dai, W. Wang, L. Hu, X. Li, J. Han, H. Wang, Y. P. Song, Z.-B. Yang, S.-B. Zheng, and L. Sun, "Demonstration of controlled-phase gates between two error-correctable photonic qubits," Phys. Rev. Lett. **124**, 120501 (2020).
24. E. Sjöqvist, D. M. Tong, L. M. Andersson, B. Hessmo, M. Johansson, and K. Singh, "Nonadiabatic holonomic quantum computation," New J. Phys. **14**, 103035 (2012).
25. M. Johansson, E. Sjöqvist, L. M. Andersson, M. Ericsson, B. Hessmo, K. Singh, and D. M. Tong, "Robustness of non-adiabatic holonomic gates," Phys. Rev. A **86**, 062322 (2012).
26. S.-B. Zheng, C.-P. Yang, and F. Nori, "Comparison of the sensitivity to systematic errors between nonadiabatic non-Abelian geometric gates and their dynamical counterparts," Phys. Rev. A **93**, 032313 (2016).
27. G. Feng, G. Xu, and G. Long, "Experimental realization of nonadiabatic holonomic quantum computation," Phys. Rev. Lett. **110**, 190501 (2013).
28. C. Zu, W.-B. Wang, L. He, W.-G. Zhang, C.-Y. Dai, F. Wang, and L.-M. Duan, "Experimental realization of universal geometric quantum gates with solid-state spins," Nature (London) **514**, 72–75 (2014).
29. S. Arroyo-Camejo, A. Lazariev, S. W. Hell, and G. Balasubramanian, "Room temperature high-fidelity holonomic single-qubit gate on a solid-state spin," Nat. Commun. **5**, 4870 (2014).
30. A. A. Abdumalikov, Jr., J. M. Fink, K. Juliusson, M. Pechal, S. Berger, A. Wallraff, and S. Filipp, "Experimental realization of non-Abelian nonadiabatic geometric gates," Nature (London) **496**, 482–485 (2013).
31. Y. Xu, W. Cai, Y. Ma, X. Mu, L. Hu, T. Chen, H. Wang, Y.-P. Song, Z.-Y. Xue, Z.-Q. Yin, and L. Sun, "Single-loop realization of arbitrary nonadiabatic holonomic single-qubit quantum gates in a superconducting circuit," Phys. Rev. Lett. **121**, 110501 (2018).
32. T. Yan, B.-J. Liu, K. Xu, C. Song, S. Liu, Z. Zhang, H. Deng, Z. Yan, H. Rong, K. Huang, M.-H. Yung, Y. Chen, and D. Yu, "Experimental realization of nonadiabatic shortcut to non-Abelian geometric gates," Phys. Rev. Lett. **122**, 080501 (2019).
33. Z. Zhang, P.-Z. Zhao, T. Wang, L. Xiang, Z. Jia, P. Duan, D.-M. Tong, Y. Yin, and G. Guo, "Single-shot realization of nonadiabatic holonomic gates with a superconducting Xmon qutrit," New J. Phys. **21**, 073024 (2019).
34. J. Q. You and F. Nori, "Superconducting circuits and quantum information," Phys. Today **58**(11), 42 (2005).
35. D. J. Egger, M. Ganzhorn, G. Salis, A. Fuhrer, P. Mueller, P. K. Barkoutsos, N. Moll, I. Tavernelli, and S. Filipp, "Entanglement generation in superconducting qubits using holonomic operations," Phys. Rev. Appl. **11**, 014017 (2019).
36. Z. Han, Y. Dong, B. Liu, X. Yang, S. Song, L. Qiu, D. Li, J. Chu, W. Zheng, J. Xu, T. Huang, Z. Wang, X. Yu, X. Tan, D. Lan, M.-H. Yung, and Y. Yu, "Experimental realization of universal time-optimal non-Abelian geometric gates," arXiv:2004.10364 (2020).
37. I. Buluta, S. Ashhab, and F. Nori, "Natural and artificial atoms for quantum computation," Rep. Prog. Phys. **74**, 104401 (2011).
38. W. Ning, X.-J. Huang, P.-R. Han, H. Li, H. Deng, Z.-B. Yang, Z.-R. Zhong, Y. Xia, K. Xu, D. Zheng, and S.-B. Zheng, "Deterministic entanglement swapping in a superconducting circuit," Phys. Rev. Lett. **123**, 060502 (2019).
39. Z.-B. Yang, P.-R. Han, X.-J. Huang, W. Ning, H. Li, K. Xu, D. Zheng, H. Fan, and S.-B. Zheng, "Experimental demonstration of entanglement-enabled universal quantum cloning in a circuit," npj Quantum Inf. **7**, 44 (2021).
40. M. A. Yurtalan, J. Shi, G. J. K. Flatt, and A. Lupascu, "Characterization of multi-level dynamics and decoherence in a high-anharmonicity capacitively shunted flux circuit," arxiv:2008.00593 (2020).
41. J. Q. You, X. Hu, S. Ashhab, and F. Nori, "Low-decoherence flux qubit," Phys. Rev. B **75**, 140515 (2007).
42. A. G. Fowler, M. Mariantoni, J. M. Martinis, and A. N. Cleland, "Surface codes: towards practical large-scale quantum computation," Phys. Rev. A **86**, 032324 (2012).
43. R. Barends, J. Kelly, A. Megrant, A. Veitia, D. Sank, E. Jeffrey, T. C. White, J. Mutus, A. G. Fowler, B. Campbell, Y. Chen, Z. Chen, B. Chiaro, A. Dunsworth, C. Neill, P. O'Malley, P. Roushan, A. Vainsencher, J. Wenner, A. N. Korotkov, A. N. Cleland, and J. M. Martinis, "Superconducting quantum circuits at the surface code threshold for fault tolerance," Nature (London) **508**, 500–503 (2014).
44. R. Barends, A. G. Fowler, A. Megrant, E. Jeffrey, T. C. White, D. Sank, J. Y. Mutus, B. Campbell, Y. Chen, Z. Chen, B. Chiaro, A. Dunsworth, I.-C. Hoi, C. Neill, P. J. J. O'Malley, C. Quintana, P. Roushan, A. Vainsencher, J. Wenner, A. N. Cleland, and J. M. Martinis, "State preservation by repetitive error detection in a superconducting quantum circuit," Nature (London) **519**, 66–69 (2015).

159.226.36.254 {ts '2021-08-26 23:02:44'}